Symmetrical Refolding of Protein Domains and Subunits: Example of the Dimeric Two-Domain 3-Isopropylmalate Dehydrogenases[†]

Éva Gráczer,[‡] Andrea Varga,[‡] Bogdan Melnik,[§] Gennady Semisotnov,[§] Péter Závodszky,[‡] and Mária Vas*,[‡]

Institute of Enzymology, Biological Research Center, Hungarian Academy of Sciences, P.O. Box 7, H-1518 Budapest, Hungary, and Institute of Protein Research, Russian Academy of Sciences, 142290 Pushchino, Moscow Region, Russia

Received October 1, 2008; Revised Manuscript Received December 20, 2008

ABSTRACT: The refolding mechanism of the homodimeric two-domain 3-isopropylmalate dehydrogenase (IPMDH) from the organisms adapted to different temperatures, *Thermus thermophilus* (Tt), *Escherichia coli* (Ec), and *Vibrio* sp. I5 (Vib), is described. In all three cases, instead of a self-template mechanism, the high extent of symmetry and cooperativity in folding of subunits and domains have been concluded from the following experimental findings: The complex time course of refolding, monitored by Trp fluorescence, consists of a fast (the rate constant varies as 16.5, 25.0, and 11.7 min^{-1} in the order of Tt, Ec, and Vib IPMDHs) and a slow (the rate constants are 0.11, 0.80, and 0.23 min^{-1} for the three different species) first-order process. However, a burst increase of Trp fluorescence anisotropy to the value of the native states indicates that in all three cases the association of the two polypeptide chains occurs at the beginning of refolding. This dimeric species binds the substrate IPM, but the native-like interactions of the tertiary and quaternary structures are only formed during the slow phase of refolding, accompanied by further increase of protein fluorescence and appearance of FRET between Trp side chain(s) and the bound NADH. Joining the contacting arms of each subunit also takes place exclusively during this slow phase. To monitor refolding of each domain within the intact molecule of *T. thermophilus* IPMDH, Trp's (located in separate domains) were systematically replaced with Phe's. The refolding processes of the mutants were followed by measuring changes in Trp fluorescence and in FRET between the particular Trp and NADH. The high similarity of time courses (both in biphasicity and in their rates) strongly suggests cooperative folding of the domains during formation of the native three-dimensional structure of IPMDH.

The folding mechanism of the most abundant multidomain or oligomeric proteins is generally very complex, scarcely investigated, and therefore barely understood (cf. reviews in refs *1* and *2*). One main question is whether domains or subunits refold independently into their native structures and associate only at a later stage of folding or whether they need to associate in order to fold properly (cf. refs *3* and *4*).

The objects of this study are variants of a dimeric two-domain protein, the enzyme 3-isopropylmalate dehydrogenase (IPMDH),[1] exhibiting different heat stabilities. IPMDH catalyzes the oxidative decarboxylation of *threo*-D-3-isopropylmalate (IPM) to 2-oxoisocaproate using NAD and divalent cation (Mn^{2+} or Mg^{2+}) as cofactors. The variants of IPMDHs are from three bacteria, the thermophilic *Thermus thermophilus* (Tt), the mesophilic *Escherichia coli* (Ec), and the psychrotrophic *Vibrio* sp. I5 (Vib) (an organism isolated from the arctic sea; cf. ref *5*. High-resolution crystal structures of Tt (*6, 7*) and Ec IPMDHs (*8*) are known, among others (*8–10*), and show a peculiar mode of association of the two subunits within the dimer (Figure 1A). No crystal structure of *Vibrio* sp. I5 IPMDH has been determined; however, a homology model has been constructed using the structure of the Ec enzyme (*11*).

Previous studies with the three (thermophilic, mesophilic, and psychrotrophic) IPMDHs have mainly dealt with the structural basis of thermal adaptation (*11–19*). We have been initiated unfolding−refolding kinetic studies with the three IPMDHs in order to explore the relationship between thermostability and the rates of unfolding and/or folding. We have established the existence a close relationship between thermostability and unfolding rate. On the other hand, the very similar folding rates of the three IPMDHs appear to be dictated by global structural characteristics (such as the highly

[†] The present publication has been prepared in the framework of the Hungarian-Russian Intergovernmental Scientific and Technological Cooperation Program and was supported by a grant (OMFB-00757/2005, Project No. RUS-15/04) from the Hungarian Foundation of Research and Innovative Technology as well as by the Ministry of Politics of Science and Technology of the Russian Federation. This international collaboration has also been supported by both the Hungarian and the Russian Academies of Sciences (Project No. 43). The financial support provided by grant OTKA NI 61915 from the Hungarian National Research Foundation as well as grants GVOP-3.2.1.2004-04 0195/3.0, HHMI N-55005607, the Russian Program for Scientific Schools N-2791.2008.4, and RFBR No. 06-04-48955 is also gratefully acknowledged.

* Corresponding author. Tel: 36 1 279 3152. Fax: 36 1 466 5465. E-mail: vas@enzim.hu.

[‡] Hungarian Academy of Sciences.

[§] Russian Academy of Sciences.

[1] Abbreviations: Tt, *Thermus thermophilus*; Ec, *Escherichia coli*; Vib, *Vibrio* sp. I5; Tf, *Thiobacillus ferrooxidans*; IPMDH, 3-isopropylmalate dehydrogenase; IPM, *threo*-D-3-isopropylmalate; IPTG, isopropyl 1-thio-β-D-galactopyranoside; ANS, 1-anilinonaphthalene-8-sulfonic acid; CD, circular dichroism; FRET, fluorescence resonance energy transfer; DSC, differential scanning microcalorimetry.

10.1021/bi801857t CCC: $40.75
Published on Web 01/20/2009

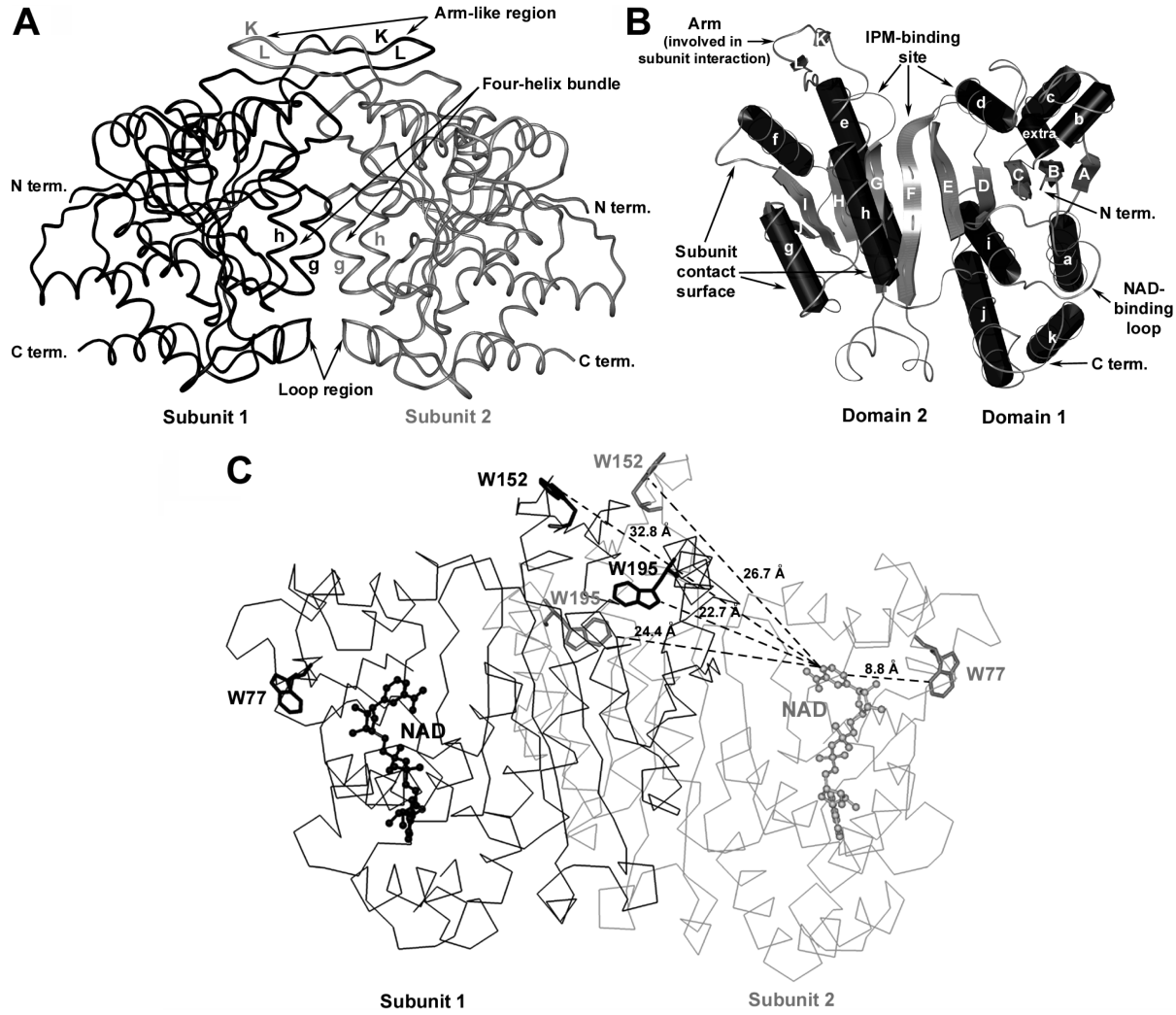

FIGURE 1: Three-dimensional structure of IPMDH. (A) Representation of the IPMDH dimer by a ribbon diagram of each subunit: subunit 1 and 2 are colored black and gray, respectively. The subunit interface is composed of a four-helix bundle (αg, αh, αg′, and αh′), a loop region on the surface of the subunit, and an arm-like region that forms an extended β-sheet with the same region of the other monomer. (B) Illustration of a single subunit of IPMDH as exemplified by the structure of the Tt enzyme (*26*) showing the arrangement and the labeling of the various secondary structural elements (according to ref *6*). (C) Positions of the cofactor NAD and the Trp residues in the structure of the IPMDH dimer. NAD and Trp molecules are represented by ball-and-stick and stick models, respectively, in the subunits of IPMDH illustrated by black and gray traces. Distances between the nicotinamide ring of NAD and the ring of Trp's are indicated.

similar native topology of the three IPMDHs) rather than by thermodynamic stability (*19*).

In the present work we are concerned about the folding mechanism of the dimeric IPMDH molecule that may not be related to the thermostability. In fact, a burst increase of protein fluorescence could be observed during refolding of all three IPMDHs, indicating formation of folding intermediate(s) (*19*). Here we investigate the question whether association of the two polypeptide chains occurs already during this burst or only at a later stage of refolding and, furthermore, whether the two domains refold simultaneously or sequentially.

The dimeric structure of IPMDHs is of special interest, since the binding site of the substrate IPM is formed by participation of side chains from both subunits (*9*). It follows, therefore, that only the dimer may possess enzyme activity. Our reactivation studies during refolding showed formation of an inactive folding intermediate in the course of the burst for all three IPMDHs (*19*). This observation would be consistent with dimer formation during only the slower phase of refolding. However, kinetic analyses of time courses of the slow part of the refolding processes clearly showed a first-order isomerization step, i.e., the absence of a second-order dimerization. Thus, this result failed to confirm the assumption about the slow association of the partially folded monomers. Therefore, the question arises whether association of the two polypeptide chains occurs during the preceding fast part of refolding. Other equilibrium denaturation (*15*) and calorimetric (*20*) studies have suggested the presence of a dimeric intermediate during the folding process. The possibility of different rate-limiting steps of the three IPMDHs of different thermal adaptabilities has to be also considered.

A further characteristic of the IPMDH structure is that each subunit contains two structural domains (Figure 1B). Domain 1 binds the coenzyme, NAD, while the substrate, 3-isopropylmalate (IPM), binds mainly to domain 2. In addition, there is a third special structural entity of the subunit, namely, an arm (consisting of two parallel β-strands, βK and βL), which strongly contributes to stabilization of the connection between the two subunits within the dimer (*6*). It is not yet clarified whether the domains (and the arm) fold cooperatively within

the subunit or independently from each other. In the latter case the polypeptide chain with a single folded domain would constitute itself a specific folding intermediate.

In order to get closer insight into the folding mechanism of IPMDH and to determine whether it is dependent on the thermostability, in the present work we have carried out systematic time-dependent renaturation experiments with the three IPMDHs of different heat adaptabilities. The extent of refolding has been detected by the spectral signals of CD, protein fluorescence, and the fluorescence energy transfer from Trp side chain(s) to the bound NADH, characteristic of the native state. For separate detection of refolding of the area located within each domain in the intact molecule, the Trp side chains (located separately in each domain) were systematically replaced in the case of Tt IPMDH with the less fluorescent Phe by site-directed mutations. From kinetic analyses registrated by different methods we could render that association of the two polypeptide chains at an early stage of refolding is a prerequisite of formation of the native three-dimensional structure of all three IPMDHs. In addition, we evidenced highly cooperative and symmetric folding of the Tt IPMDH domains as well as that proper folding and joining the two arms occur only during the later slow stage of refolding. This feature of folding, however, seems to be generally valid for all IPMDHs, independent of their thermal stability.

MATERIALS AND METHODS

Reagents. threo-DL-3-Isopropylmalic acid (IPM) was purchased form Wako Biochemicals (Japan); NAD and NADH were Boehringer Mannheim products. Isopropyl 1-thio-β-D-galactopyranoside (IPTG) (Fermentas), chloramphenicol, and ampicillin (Sigma) were used for fermentation. Chromatography media were obtained from GE Healthcare. All other chemicals (high purity grade) were products of Merck, Reanal, and Sigma.

Enzyme Expression and Purification. The non-His-tagged variants of Tt and Vib IPMDHs as well as the His-tagged variants of Tt and Ec IPMDHs were expressed and purified as described earlier (*19*). Briefly, for purification ammonium sulfate fractionation as well as DE52 anion-exchange, butyl-Sepharose hydrophobic, DEAE-Sepharose anion-exchange, and Sephacryl S-200 gel chromatographic steps were subsequently applied, based on previous publications (*14, 21*). His-tagged variants of Tt and Ec enzymes were purified by Ni^{2+} affinity chromatography using 120 mM imidazole for elution. The following mutants of Tt IPMDH have been prepared by site-directed mutagenesis, W152F, W77,152F, and W152,195F, and were expressed and purified similarly to the wild-type enzyme. The purified enzyme solutions at a concentration of 5−10 mg/mL were frozen in liquid nitrogen and stored at −80 °C.

Site-Directed Mutagenesis. The side chains of W77, W152, and W195 of Tt IPMDH were mutated into phenylalanine using the QuickChange site-directed mutagenesis kit (Stratagene). The primers were the following: W77F, forward 5′-GTGGGGGGGCCCAAG**TTC**GACGGCCTTCCCCGC-3′, reverse 5′-GCGGGGAAGGCCGTC**GAA**CTTGGGCC-CCCCCAC-3′; W152F, forward 5′-CGAGGCCGAGGCC-**TTC**AACACGGAGCGCTAC-3′, reverse 5′-GTAGCGCTC-CGTGTT**GAA**GGCCTCGGCCTCG-3′; W195F, forward 5′-CGAGGTGGGAGAGTTC**TTC**CGCAAGACCGTGGA-GGAGG-3′, reverse 5′-CCTCCTCCACGGTCTTGCG**GAA**-GAACTCTCCCACCTCG-3′. The mutations were checked by DNA sequencing.

Determination of Protein Concentration and Enzyme Activity. Protein concentration was determined from the UV absorption at 280 nm. The molar absorption coefficients of 47900 for the wild-type Tt and 54780 $M^{-1}\cdot cm^{-1}$ for Ec or Vib IPMDH, respectively, are calculated for the dimers from the amino acid contents using the formula given by Pace and co-workers (*22*). The same type of calculation resulted in 36900 for the single mutant W152F and 25900 $M^{-1}\cdot cm^{-1}$ for the double mutants W77,152F and W152,195F of the Tt enzyme, respectively. The molecular masses of the non-His-tagged variants of Tt, Ec, and Vib IPMDHs were taken to be 73300, 78780, and 76960 Da, respectively. The presence of a His tag caused an additional increase of all molecular masses by 1430 Da.

The activity of IPMDH (6−12 μg/mL, i.e., 0.08−0.16 μM) was assayed in the presence of 0.6 mM IPM, 3 mM $MgCl_2$, and 1.4 mM NAD in 20 mM KH_2PO_4−KOH buffer, pH 7.6, containing 300 mM KCl and 10 mM DTT. The formation of NADH was recorded spectrophotometrically at 340 nm. The measurements were carried out using a Jasco V-550 spectrophotometer (Japan, Tokyo) equipped with a Grant Y6 thermostat. The molar activities of Tt, Ec, and Vib IPMDHs in the same order were 380 ± 50, 1180 ± 150, and 1350 ± 150 min^{-1}. The mutants of W152F and W77,152F of Tt IPMDH exhibited similar activities to its wild-type form. The mutant of W152,195F, however, had no initial enzyme activity, but it was restored to up to 195 min^{-1} upon 1 h preincubation with the substrate, IPM.

Time-Dependent Refolding Experiments. For renaturation studies, denatured Tt, Ec, or Vib IPMDHs were prepared at protein concentrations of 600 μg/mL (i.e., 8.15 μM) upon incubation for 24 h, 1 h, or 10 min, respectively, in 20 mM KH_2PO_4−KOH buffer, pH 7.6, containing 8.5 M urea, 300 mM KCl, and 10 mM DTT. It was checked that omission of KCl from the buffer did not influence the experimental results. Refolding experiments were initiated by 10−100-fold dilution of the denatured protein into the same phosphate buffer, containing no urea, using either a magnetic stirrer (dead time 1 s) or stopped-flow attachment (Unisoku Inc., Japan) for monitoring of slow or fast parts of refolding. The final protein concentration of the renaturation mixtures varied from 6 to 120 μg/mL (i.e., 0.08−1.63 μM). Time courses of refolding were followed at 20 °C by the methods described below.

The extent of refolding varied between 50% and 70% for all three enzymes independent of methods used for detection.

Circular Dichroism Measurements. CD measurements were performed on a Jasco J-720 spectropolarimeter (Japan) equipped with a Neslab RTE 111 computer-controlled thermostat. For recording of far-UV CD spectra, the cuvette with 0.1 mm path length was used at a protein concentration of 1 mg/mL (13.6 μM). To monitor the slow phase of the protein refolding, the standard cuvette with 10 mm path length and manual mixing were used at a final protein concentration of 0.01 mg/mL (136 nM). For recording near-UV CD spectra a standard cuvette with 10 mm path length was used at a protein concentration of 3.8 mg/mL (50 μM). All measurements were carried out at 20 °C.

Protein Fluorescence Measurements. The changes of protein fluorescence during refolding were recorded using a SPEX Fluoromax-3 spectrofluorometer equipped with a Peltier thermostat (Edison, NJ). The samples were excited at 275 or 295 nm, and the emission was monitored at 335 nm using the cuvette with 10 × 10 mm path lengths. The slits of 2 nm and 2 or 4 nm were applied for excitation and emission, respectively, depending on the actual protein concentration.

In some cases the initial phase of the refolding time course was followed by stopped-flow equipment with the dead time of 5 ms.

Fluorescence Polarization Measurements. When refolding was followed by measuring Trp fluorescence, the values of fluorescence polarization were also recorded as a function of time. The fluorescence anisotropy values were calculated using the equation:

$$\langle r \rangle = \frac{I_{VV} - GI_{VH}}{I_{VV} + 2GI_{VH}} \quad (1)$$

where $G = I_{HV}/I_{HH}$, I is the fluorescence signal, while the first subscript indicates the position of the excitation of polarizer and the second, the emission polarizer (*23*).

Fluorescence Energy Transfer Measurement. The fluorescence energy transfer between Trp(s) of IPMDH and the bound NADH was detected in the presence of IPM, as reported by Dean and Dvorak (*24*). The usual mixture contained 12 μg/mL IPMDH (0.16 μM dimer concentration), 12.5 μM NADH, 3 mM $MgCl_2$, and 0.6 mM IPM. These conditions were applied when the refolding time course was followed by detecting the occurrence of energy transfer, i.e., formation of the emission band of the bound NADH at 410 nm upon excitation of Trp fluorescence of IPMDH at 295 nm, characteristic of the native state of the enzyme.

Determination of the Binding Constant of IPM to Native IPMDH and during Its Refolding. IPM binding to the complex of native IPMDHs (Tt, Ec, and Vib) with NADH was detected by fluorometric titration using the signal of FRET occurring between the protein Trp's and the bound NADH, upon addition of increasing concentrations of IPM (cf. Figure 5E).

Formation of the IPM binding site during the time courses of refolding of Tt, Ec, and Vib IPMDHs was detected by following the formation of the FRET signal in the presence of different concentrations of IPM. From these series of time courses, the FRET intensities, measured at different given time intervals of refolding, are plotted against the applied IPM concentrations. By this way we constructed the IPM titration curves at different given extents of refolding. From these curves changes in the K_d values of IPM binding during refolding could be obtained (cf. Figure 5F).

Differential Scanning Calorimetry (DSC) Experiments. The measurements were carried out in a MicroCal VP-DSC type microcalorimeter (MicroCal Inc.) with a cell volume of 0.51 mL, at constant scan rate of 60 °C/h in 20 mM KH_2PO_4−KOH buffer, pH 7.6, containing 300 mM KCl. In all experiments carefully degassed samples were used, and the protein concentration was constant at 0.5 mg/mL (6.8 μM). The data were analyzed using MicroCal Origin 5.0 software.

Native Gel Electrophoresis. Native gel electrophoresis was performed according to Orstein and Davis (*25*). The resolving and stacking gel was 10% and 5%, respectively. IPMDH (2.7 μg) was loaded into the gel, and the electrophoresis was carried out at 180 V for 1 h on ice.

Molecular Graphics Analysis. The subunit−subunit and domain−domain contacts were analyzed by the aid of molecular graphics using the known crystal structures of Tt (PDB entries 1XAA (*26*) and 1HEX (*7*)) and Ec (PDB entry 1CM7 (*8*)) IPMDHs. In addition, the three-dimensional homology model of Vib IPMDH (*11*), kindly provided by the authors, was used for similar analysis.

To analyze the conformational changes caused by IPM binding, the structure of Tf IPMDH (PDB entry 1A05 (*9*)) was surveyed in comparison with the IPM-free structure of Tt IPMDH that binds NAD (PDB entry 1HEX (*7*)).

For visualizing the molecular contacts, INSIGHT II (Byosim/MSI, San Diego, CA) was used. The distance limits for hydrogen bonds, hydrophobic interactions, and ionic interactions were 3.5, 4.5, and 4.0 Å, respectively.

RESULTS AND DISCUSSION

Nature of the Early Kinetic Intermediate during Refolding of IPMDHs. We have shown previously that the refolding time courses of all three investigated IPMDHs are biphasic processes occurring at similar time scales (*19*). These observations have led to the conclusion that the mechanism of refolding may not be related to the thermostability. Here we demonstrate that for all three enzymes the biphasic process includes an initial burst of at least 90% of the total change, if followed by recording far-UV CD (Figure 2A,B). Thus, formation of the secondary structure occurs at the very beginning of refolding, indicating the presence of at least one folding intermediate. In agreement, a molten globule-like intermediate state (with fully formed secondary structural elements) has been detected for all three IPMDH species using the protein-bound hydrophobic probe ANS (*19*). In contrast to the CD measurements, the burst is much smaller, about 25 or 50% of the total change (depending on the enzyme form, due to their different Trp contents) if followed by measuring protein fluorescence (Figure 2C,D). It is notable, however, that the absolute amplitude of this burst is the same for all three IPMDHs. Since Trp 152 (located in the arm region of the Tt enzyme) is absent in the structures of Ec and Vib IPMDHs, it follows that Trp 152 solely contributes to the slow part of the fluorescence change. Furthermore, previously we have observed an initial lag phase, if refolding was followed by measuring the recovered activity (*19*). These observations suggested the presence of an inactive but already native-like early intermediate during the folding pathway, with the secondary structure content close to the native state. The native-like character of the intermediate is also reflected by its spectral properties (λ_{max} of its emitted spectrum is already red shifted and coincides with that of the native enzyme), as illustrated in Figure 2D, where spectra of the unfolded, refolded, and intermediate states are shown for Tt IPMDH. Similar types of spectral changes were registered also for Ec and Vib IPMDHs (not shown). This observation allows us to conclude that Trp residues of the protein in the burst intermediate state are essentially desolvated, but the fluorescence intensity is still far from native level, indicating that the native environment of Trp residues is not fully formed in the intermediate.

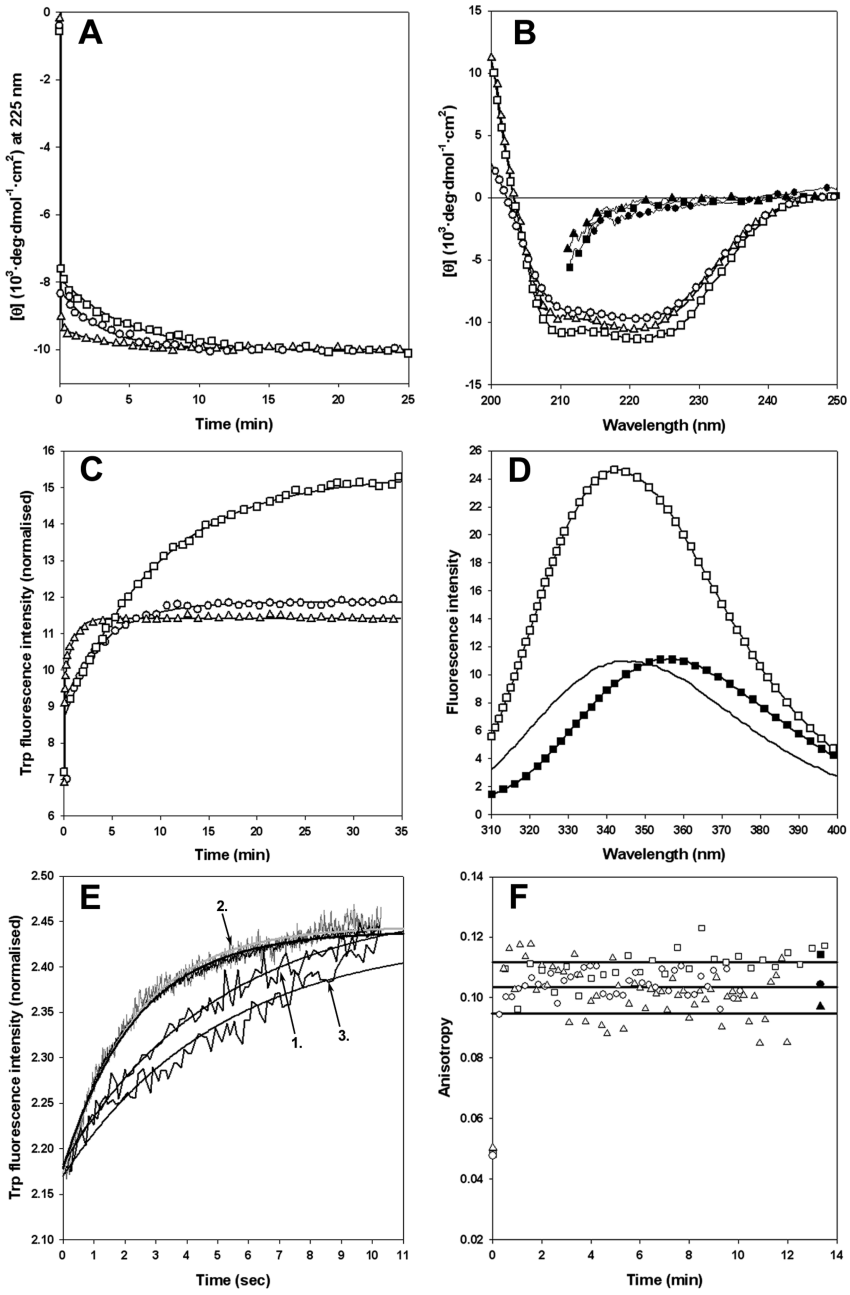

FIGURE 2: Renaturation kinetics of the IPMDHs. (A) Formation of the secondary structure of Tt (□), Ec (△), and Vib (○) IPMDHs was monitored by far-UV CD spectroscopy (λ = 225 nm) at an enzyme concentration of 136 nM. (B) The CD spectra of the native and denaturated Tt (□, ■), Ec (△, ▲), and Vib (○, ●) IPMDHs are represented by empty and filled symbols, respectively. (C) Time courses of Tt (□), Ec (△), and Vib (○) IPMDHs were followed by Trp fluorescence, and the first-order rate constants of the slow parts obtained in the same order are 0.11 ± 0.02, 0.80 ± 0.20, and 0.23 ± 0.03 min^{-1} (data from ref *19*). The enzyme concentration was 163 nM. (D) The spectrum of the intermediate (solid line) was recorded at 30 s after initiation of refolding, and its λ_{max} coincided with that of the native Tt IPMDH spectrum (□). The spectrum of the denaturated Tt IPMDH is shown by comparison (■). (E) Time courses of the fast (burst) part of renaturation for Tt (1), Ec (2), and Vib (3) IPMDHs monitored by fluorescence stopped flow. It cannot be excluded that the amplitude of this fast part is somewhat smaller than the complete burst shown in panel C due to the uncertainties of the baseline of the stopped-flow instrument. In all cases the measurements were carried out at two different enzyme concentrations, but this is only illustrated in the case of the Ec enzyme: 2.45 μM (black trace) and 0.27 μM (gray trace). The rate constants of 16.5 ± 3.7, 25.2 ± 5.1, and 11.7 ± 2.8 min^{-1} were obtained by fitting the curves to a single exponential. (F) Fluorescence anisotropy was monitored during refolding of Tt (□), Ec (△), and Vib (○) enzymes at a concentration of 163 nM. Filled symbols represent the anisotropy of the native enzymes. The excitation was carried out at 275 nm in all cases.

Concerning the fluorescence intensity increase upon renaturation, besides changes in λ_{max}, it reflects an average of the native environments of all individual Trp side chains. Surveying the literature there are examples of both increase (*27–29*) and decrease (*30–32*) of intensities of protein fluorescence upon refolding. Up to now, however, it is basically impossible to predict correctly how the fluorescence intensity will change upon unfolding−refolding (*33*).

In order to check the association state (monomer or dimer) of the IPMDH refolding intermediate, we have studied protein concentration dependences of both the burst and the slow parts of the refolding process. Earlier

we found that the rate of the slow part of refolding did not depend on protein concentration in a wide range (from 6 to 120 μg/mL); thus a second-order process (e.g., dimerization) as a rate-limiting step could be excluded during the slow phase (*19*).

Therefore, we assumed that the dimerization process (i.e., the association of the two polypeptide chains) occurs during the burst. Here we investigated the protein concentration dependence of the burst using fast kinetic detection of the change in protein fluorescence. The experiment carried out with all three IPMDHs gave very similar stopped-flow kinetic traces. Moreover, in contrast to the expectation, no protein concentration dependence was observed, as illustrated by the experiment with Ec IPMDH at two greatly different protein concentrations (gray and black traces and fitted curve 2 in Figure 2E). Thus, again a simple first-order isomerization could be concluded, although the second-order association step of the two polypeptide chains must occur within the folding pathway. The only possibility is that this second-order step, although takes place, it is not rate limiting at any phase of refolding. Closely similar time courses were observed for the Tt (curve 1) and Vib (curve 3) IPMDHs as well as for the mutants of Tt IPMDHs, studied below (not shown).

In the following we used measuring Trp fluorescence anisotropy that is sensitive to both an intramolecular mobility of Trp residues and rotation of protein molecule as a whole (*34*). Because the hydrodynamic volume of the protein molecule is essentially increased upon dimerization, one can expect the increase of Trp fluorescence anisotropy if protein dimerization occurs. It was found that, after a burst increase, the anisotropy value did not change further during the slow phase of IPMDH refolding and corresponded to the value characteristic to the native dimers for all of the Tt, Ec, and Vib enzymes (Figure 2F). Although changes in the fluorescence lifetimes cannot be excluded during association of the monomers, it is very much improbable that the changes of the lifetime (if there is any) and the changes of the hydrodynamic volume were exactly compensating each other. Moreover, the increase of Trp fluorescence intensity during the slow phase of Ec or Vib IPMDH refolding is much less than that for the Tt one (Figure 2C), but the increase of anisotropy during this phase is absent for all three proteins (Figure 2F). Therefore, we argue in favor of the presence of an associated dimeric form (probably in a molten globule state at the beginning) throughout the slow phase of refolding. Another characteristic of the folding intermediate is that the ability of the initial, non-native-like interaction with IPM, demonstrated in a separate section below, is entirely consistent with the conclusion about its dimeric state. Accordingly, association of the two polypeptide chains most probably occurs during the burst process and provides a prerequisite of the further slower part of refolding.

Simultaneous Refolding of IPMDH Domains As Revealed by Refolding Studies with the Trp Mutants. The Tt IPMDH polypeptide chain contains three tryptophan residues, W77, W152, and W195. In the spatial structure of IPMDH W152 is placed within the arm-like region which participates in intersubunit interaction (Figure 1B,C), while W77 and W195 are located in separate domains, domain 1 and domain 2, respectively. In order to study refolding of selected areas separately within the protein molecule, we have systematically replaced the Trp residues of Tt IPMDH with the much less fluorescent Phe by site-directed mutagenesis. The constructed single mutant W152F and the double mutants W77,152F and W152,195F were first tested by their CD spectra. The far-UV CD spectra were indistinguishable from that of the wild-type Tt enzyme (not illustrated). On the other hand, the near-UV CD spectra were characteristic of the individual Trp mutants, and only the spectrum of the protein bearing a single mutation in the arm-like region (W152F) corresponds to the spectrum of the wild-type Tt IPMDH (Figure 3A). The spectra of the two double mutants (W152,77F and W152,195F) are strikingly different from each other, not only in their intensities but also in their $\pm$ signs, indicating that the native environments of Trp 77 and Trp 195 are very different from each other. When the spectra of the two double mutants are summarized, the resulting spectrum corresponds to that of the wild-type enzyme (Figure 3A). This additivity of the spectra argues in favor of the native-like surroundings of Trp's in each mutant. Furthermore, in DSC experiments the cooperative calorimetric transition of the wild-type enzyme is more or less preserved for the mutants, except for the mutant W152,195F, where the transition is much less cooperative, and its T_m value is also considerably decreased (Figure 3B). It is also notable that this mutant exhibits ANS-binding ability, in contrast to the native wild-type enzyme, which does not bind ANS at all (not shown). This is consistent with the less compact structure of this mutant. The native gel electrophoretic mobilities of the mutants also sensitively followed even the small changes observed in the DSC runs (Figure 3C). Enzyme activity tests of the mutants also clearly revealed preservation of the native structures for W152F and W77,152F mutants. However, the mutant W152,195F initially did not exhibit enzyme activity but was considerably activated after incubation in the activity assay mixture. We have found that an $\sim$1 h preincubation with a saturating concentration of IPM was effective in restoring most of the native enzyme activity for this mutant.

Thus, in spite of the findings that mutations of Trp residues influence on the protein thermostability and hydrodynamic volume, IPMDH mutants contain the majority of structural elements in the native-like conformation.

Figure 4A represents fluorescence spectra of wild-type Tt IPMDH and its Trp mutants in the native and unfolded states. The spectra of the proteins in the unfolded state show the expected decrease in the intensity that is proportional to the number of Trp residues in the protein polypeptide chain. On the other hand, the spectra of the protein in the native state allow us to evaluate the contribution of different Trp residues in fluorescence of the structured protein molecule. The smaller contribution has Trp 77, the fluorescence intensity of which is practically equal to that in the unfolded state. The environment of Trp 195 has been displayed in more high fluorescence intensity in comparison with unfolded state. On the other hand, as expected for the W152F mutant that lacks Trp 152 (cf. Figure 1C), its protein fluorescence intensity is further increased.

Figure 4B represents refolding kinetics of the wild-type protein and its Trp mutants monitored by restoration of Trp fluorescence at 335 nm. It is clear that the mutants exhibited kinetic behavior (including both the presence of the burst and the rates of the slow phases) very similar to each other

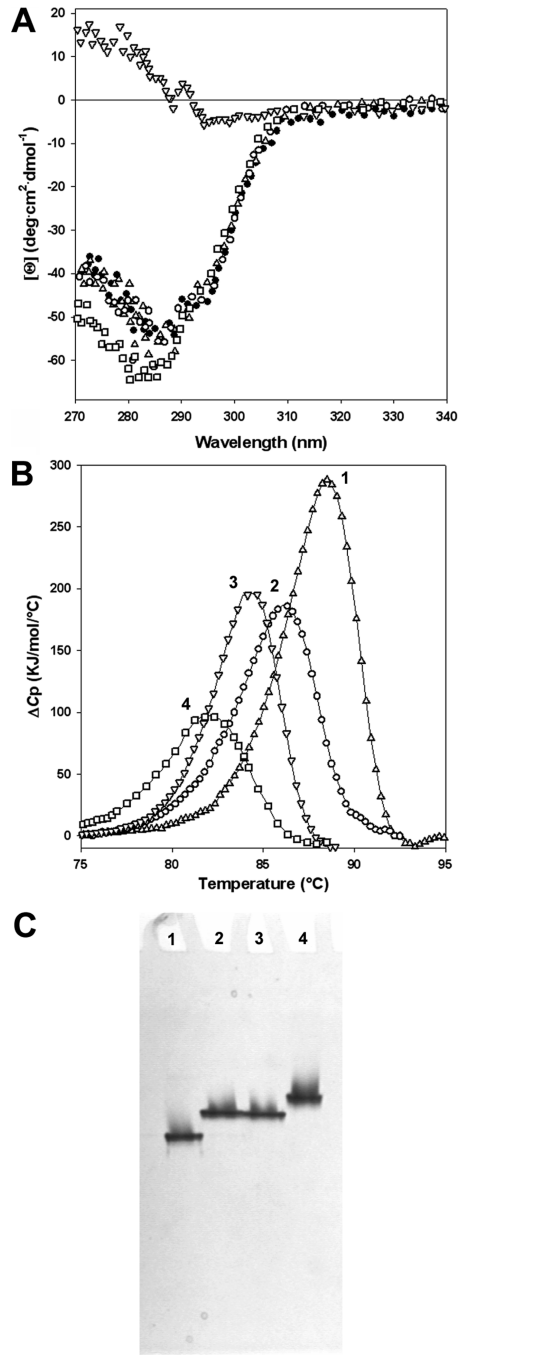

FIGURE 3: Effects of mutation on the tertiary structure (A), thermal stability (B), and hydrodynamic volume (C) of Tt IPMDH. (A) The presence of the tertiary structure were monitored by recording the near-UV CD spectra of wild-type (△), W152F (○), W152,77F (▽), and W152,195F (□) Tt IPMDHs at an enzyme concentration of 50 μM. The sum of the spectra of W152,77F (▽) and W152,195F (□) is indicated by the filled symbols (●). (B) DSC heat transition curves were determined with the same protein forms as in panel A. The T_m values obtained are 88.5 ± 0.2, 86.1 ± 0.1, 84.4 ± 0.3, and 82.1 ± 0.2 °C, in the order of wild type (△, 1), W152F (○, 2), W152,77F (▽, 3), and W152,195F (□, 4) Tt, respectively. (C) Native gel electrophoresis was carried out also with the same protein forms.

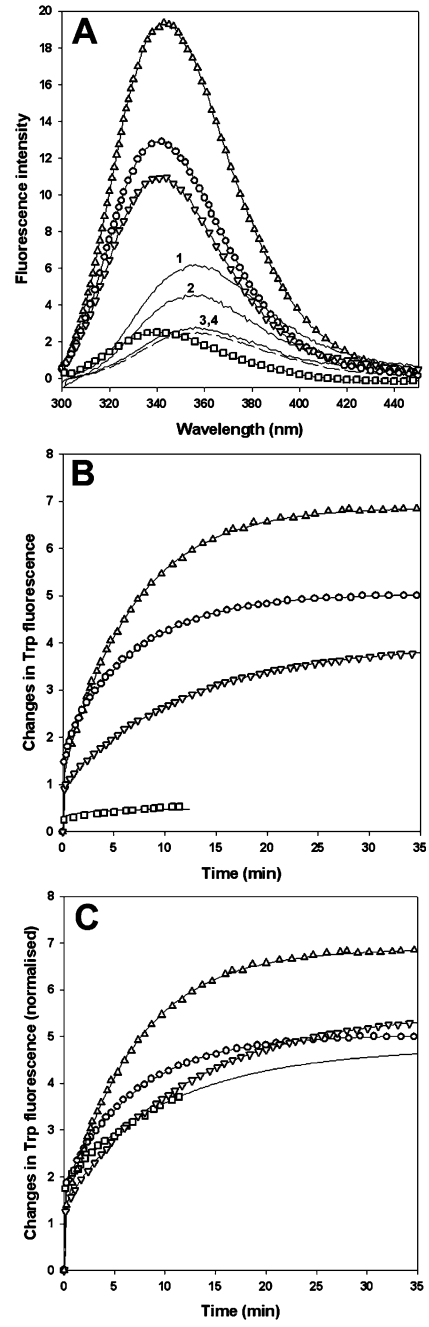

FIGURE 4: Comparison of the renaturation kinetics of the mutant IPMDHs followed by Trp fluorescence. Spectra of the native and denatured forms of wild-type (△, 1), W152F (○, 2), W152,77F (▽, 3), and W152,195F (□, 4) IPMDHs are represented in panel A. Panel B shows the time courses of renaturation of wild-type (△), W152F (○), W77,152F (▽), and W152,195F (□) IPMDHs. The rate constants, in the same order, are the following: 0.11 ± 0.02, 0.12 ± 0.02, 0.078 ± 0.010, and 0.24 ± 0.10 min^{-1}. In panel C the time courses of W77,152F and W152,195F IPMDHs were normalized to that of W152F using the factor derived from the spectra of their native forms, as well as taking into account the slight differences observed in the extent of their renaturation. The excitation occurred at 295 nm in all cases.

and to that of the wild-type enzyme. This similarity becomes even more evident after normalization of the kinetic runs (Figure 4C). Since the double mutants contain a fluorescent Trp side chain in either domain 1 or domain 2, the kinetics reflect refolding of their local environments in either domain 1 or domain 2. No substantial difference between these refolding time courses could be observed, providing clear evidence for the simultaneous and possibly cooperative refolding of the two domains within the intact molecule.

Regarding the refolding kinetics of the single mutant that lacks Trp 152 in the arm region of the subunit, it is remarkable that this mutation causes a significant decrease in the amplitude of only the slow part of refolding, without

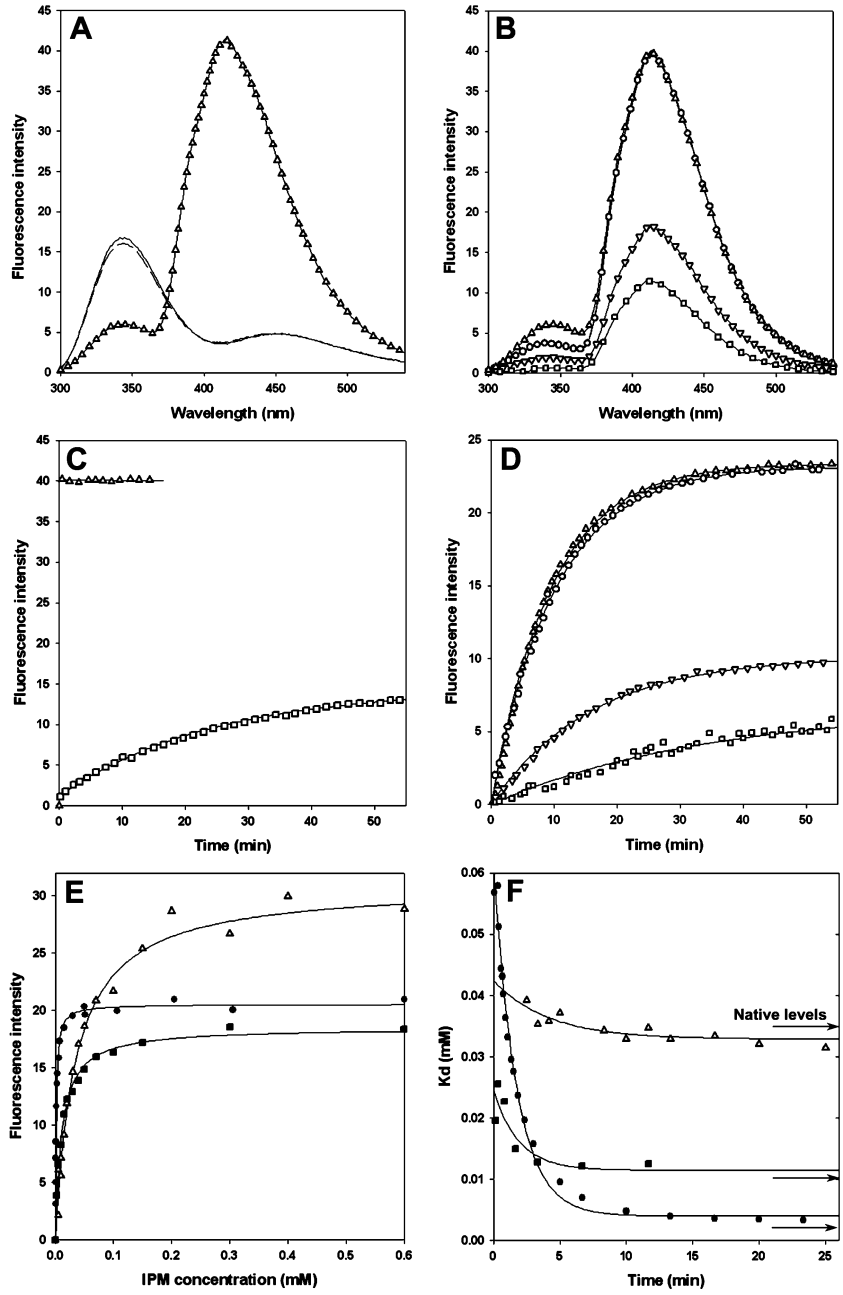

FIGURE 5: Comparison of the renaturation kinetics of wild-type and mutant Tt IPMDHs as well as IPM binding to Tt, Ec, and Vib IPMDHs as detected by fluorescence resonance energy transfer (FRET). (A) The solid line shows the fluorescence spectrum of the native wild-type Tt IPMDH complexed with NADH. The dashed line represents the effect of $MgCl_2$ added to the solution. Upon addition of IPM the spectral changes characteristic of FRET appeared (△). (B) Comparative FRET spectra of wild-type and mutant Tt IPMDHs in their native states: wild type (△), W152F (○), W77,152F (▽), and W152,195F (□). (C) Time courses of the appearance of FRET for the native wild-type Tt IPMDH (△) and for the mutant Tt W152,195F (□) after addition of IPM to the enzymes. The rate constant of the latter process is 0.067 ± 0.008 min^{-1}. (D) The appearance of the FRET signal during renaturation of the wild-type (△), W152F (○), W77,152F (▽), and W152,195F (□) Tt IPMDHs. The rate constants, in the same order, are 0.11 ± 0.02, 0.10 ± 0.02, 0.066 ± 0.010, and 0.033 ± 0.004 min^{-1}, respectively. (E) IPM binding to the complex of native IPMDH−NADH binary complex was monitored by recording the appearance of the FRET signal upon addition of increasing concentrations of IPM to Tt (△), Ec (■), and Vib (●) IPMDHs. The K_d values of 34.1 ± 2.3, 10.9 ± 0.7, and 1.3 ± 0.1 μM were derived by computer fitting of the experimental curves. (F) Changes in the K_d values of IPM binding during refolding (cf. Materials and Methods). Arrows at the right-hand ordinate represent the K_d value characteristic for the native state. In all experiments the measurements were performed at 0.16 μM (12 μg/mL) IPMDH, 12 μM NADH, 3 mM $MgCl_2$, and 0.6 mM IPM concentrations.

influencing the amplitude of the burst part (Figure 4B). The refolding time course of this mutant is comparable with that of the Vib enzyme which also lacks the equivalent nonconserved Trp (Figure 2C). This means that proper folding of the arm and possibly the native-like contacts between them are only formed during the slow part of refolding. These contacts further strengthen the contacts between the subunits, i.e., further stabilize the dimeric structure that is initially formed during the burst.

Restoration of IPM Binding and the IPM Stabilized Conformation As Reflected by Appearance of FRET during Refolding. It was noted earlier that spectral changes, characteristic of FRET from the Trp side chain(s) of IPMDH to the protein-bound NADH are taking place but, interestingly,

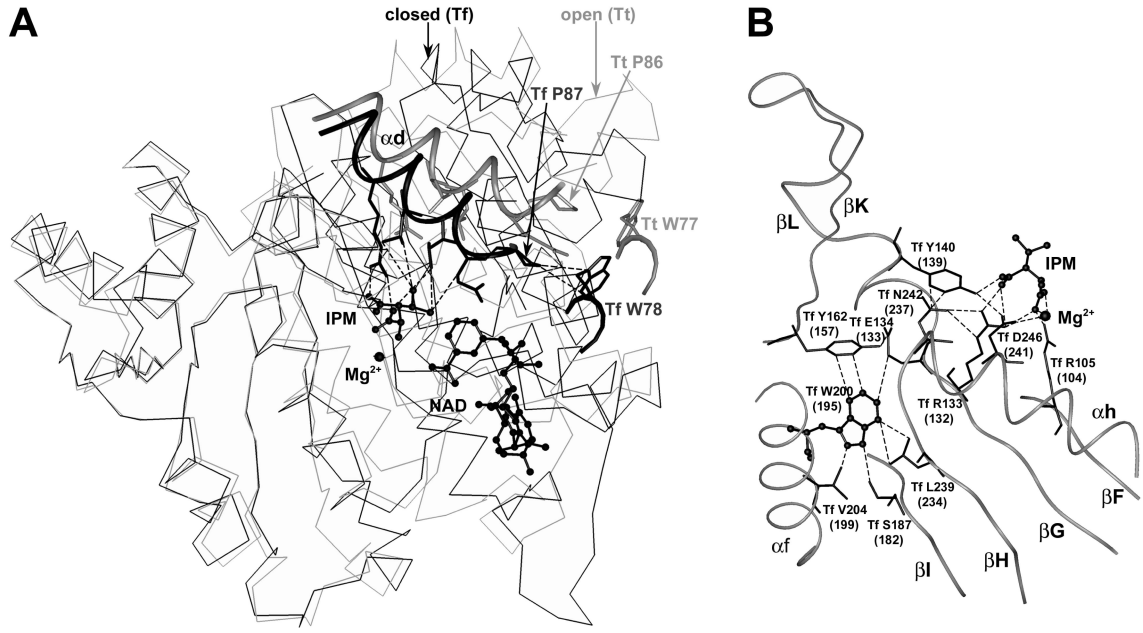

FIGURE 6: Effect of IPM binding on the conformation of IPMDH. (A) The subunits of Tt (open) and Tf (closed) IPMDHs are superimposed according to the inner β-strands of domain 2 and colored by gray and black, respectively. IPM binds only to Tf IPMDH, while NAD is bound originally to the open crystal structure of Tt IPMDH. In order to deduce the possible position of the bound NAD molecule in the closed IPM-bound structure (i.e., to model the ternary complex), a subunit of Tt IPMDH (not shown, except its NAD molecule) was superimposed with a subunit of Tf IPMDH, but at this time according to domain 1. Both the bound IPM and the graphically positioned NAD molecules are represented by black ball-and-stick models and the indicated side chains by stick models. Helix αd is highlighted by ribbons. (B) Communication between surroundings of W195(Tt)/W200(Tf) and IPM (ball-and-stick models) sites is represented by tertiary interactions of certain conserved side chains (stick models). The indicated secondary structural elements are shown by ribbons. The tertiary contacts are indicated by dashed lines.

only if the substrate IPM is also bound (*24*). The spectra in Figure 5A illustrate this phenomenon in the case of Tt IPMDH: a new emission band of the NADH (acceptor) bound to IPMDH around 410 nm appeared with a concomitant decrease of the emitted protein (Trp) fluorescence (donor) around 340 nm, upon addition of IPM to the binary complex of IPMDH and NADH. It is well-known that Trp and NADH are a good donor−acceptor pair with characteristic distance $R_0 \approx 25$ Å for 50% efficiency of energy transfer in case of favorable orientation of their electronic dipoles (*35*). The crystal structure of IPMDH (Figure 1C) shows that the distances between the indole group of any of the Trp residues and the nicotinamide ring of the bound NAD (and hence NADH) would be sufficient for effective energy transfer, even in the absence of bound IPM. We have checked with the X-ray coordinates of Tf IPMDH that these distances are somewhat further shortened in the presence of bound IPM, possibly due to domain closure (depicted in Figure 6A) accompanying IPM binding. Thus, although the Trp's do not interact directly with IPM, it is possible that the protein conformational changes that accompany IPM binding optimize both position and orientation of the Trp side chains relative to the bound coenzyme. In this respect only W77 and W195 should be considered as responsible ones, since the FRET spectra of the Trp mutants (Figure 5B) have excluded the role of W152 as a possible donor for FRET, probably due to improper orientation of its side chain regarding the nicotinamide ring of NADH.

Surveying the molecular contacts of the two responsible Trp's in relation to IPM binding provided a reasonable structural explanation for the appearance of FRET upon binding of IPM. Figure 6A illustrates that the terminus of helix αd (bearing IPM binding side chains) moves about 6 Å distance upon domain closure. Thereby Pro 86 at the N-terminus of αd also moves for the same distance. Since P86 (or the equivalent P90 and P88 in the Ec and Vib enzymes, respectively) is directly contacted with the ring of W77 through apolar interactions, the side chain of W77 also moves. Due to this movement W77 is shifted a little closer to the nicotinamide ring, but, more importantly, its ring is rotated by about 40−45° compared to its original position and thereby optimizes its orientation for the effective FRET. Thus, the FRET signal of W77 reports about formation of the domain-closed conformation.

As for W195, its side chain is involved in a network of tertiary interactions with the same secondary structural elements (αh, βF, βG, βH, and βI) to which IPM itself interacts (Figure 6B). Furthermore, the other IPM molecule bound to the other subunit (not shown) interacts with Val 188 at the N-terminus of helix αf, i.e., the same helix that bears Trp 195. Thus, IPM binding to either subunit can affect the position of Trp 195. Therefore, the FRET signal of W195 (in contrast to the much smaller FRET signal of W77) reports about formation of both subunit−subunit and domain−domain interactions.

Because FRET appears very fast (within 1 s) after addition of IPM and NADH to native IPMDHs (shown by the upper time course in Figure 5C), it is possible to monitor the slow phase of the protein refolding by FRET (here there is no burst phase; see Figure 5D). One can see that the refolding kinetics of the wild-type Tt IPMDH recorded by FRET is very similar to the slow phase of the time course recorded by Trp fluorescence (cf. Figure 2C). It means that formation of the proper geometry of the IPM binding site occurs simultaneously with formation of the native tertiary structure.

Table 1: List of Molecular Contacts at the Subunit−Subunit Interfaces of the Investigated IPMDHs[a]

Tt	Ec	Vib	secondary structural elements	nature of interaction
P117-R225	P122-I234	S119-V231	loop βF-βG, αg′	hydrophobic
L118-V224	L123-I234	L120-V231		
K119-K119	R124-R124	K121-K121	loops βF-βG, βF′-βG′	
Y139-V188	**Y145-V198**	**Y141-V195**	loops βG-βK,	
Y139-L189	**Y145**-L199	**Y141**-L196	βI′-αf′	
A149-S158	E159-H168	R156-S165	loop βK-βL, βL′	
R144-**V188**	K150-**V198**	R146-**V195**	βK, loop βI′-αf′	H-bond
R144-E190	−	−		salt bridge
−	K150-Q200	−		hydrophobic
G145-E190	G151-Q200	Q147-A197		
M146-E190	−	−	βK, αf′	
M146-E193	−	−		
M146-F194	−	−		
−	Q157-R169	−	loop βK-βL, αe′	
−	Q157-F170	−		
	E159-R169	R156-E166		salt bridge
A149-K159	E159-R169	R156-E166		H-bond
A151-**Y157**	A161-**Y167**	A158-**Y164**	βL, βL′	
N153-E155	D163-E165	D160-L162		
E150-S158	K160-H168	M157-S165		hydrophobic
W152-R156	F162-V166	Y159-P163		
E150-F194	K160-L204	M157-L201	βL, αf′	
A151-E190	A161-Q200	A158-A197		
A151-F194	A161-L204	A158-L201		
N153-L189	D163-L199	D160-L196	βL, loop βI-αf′	
N153-E190	D163-Q200	D160-A197	βL, αf′	hydrophobic, H-bond
N153-V191	D163-S201	D160-S198		H-bond
V216-I242	I226-I252	V223-I249	αg, αh′	hydrophobic
A220-I242	T230-I252	A227-I249		
M221-**D245**	M231-**D255**	M228-**D252**		
M221-V249	M231-M259	M228-M256		
R225-V249	K235-M259	R232-M256		
V224-V224	I234-I234	V231-V231	αg, αg′	
I238-**F239**	L248-**F249**	L245-**F246**	αh, αh′	

[a] The atomic contacts were deduced from the known X-ray structures as described in Materials and Methods. Residue numbering corresponds to the known sequence numbering. Structurally equivalent contacts are listed on the same line. Conserved residues are indicated in bold.

Table 2: List of Molecular Contacts at the Domain−Domain Interfaces of the Investigated IPMDHs[a]

Tt	Ec	Vib	secondary structural elements	nature of contact
A101-L262	S106-L272	G103-L269	βF and βE	H-bond
N102-A260	N107-A270	N104-A267		
L103-A260	L108-A270	L105-A267		
A101-S261	S106−S271	G103-S268	βF and βE	hydrophobic
N102-A260	**N107**-A270	**N104**-A267		
N102-A261	N107−S271	N104−S268		
L103-A260	L108-A270	L105-A267		
L103-L262	L108-L272	L105-L269		
R104-S259	**R109-S269**	**R106-S266**		
P105-P258	**P110**-P268	−		
−	−	**R106**-L264		
−	−	**P107**-L264		
−	A111-L267	A108-L264		
L103-M296	−	L105-M304	βF and αi	hydrophobic
P105-M296	**P110**-L307	**P107**-M304		
L103-H300	L108-Y311	L105-Y308		
R104-V272	**R109**-A283	**R106**-C280	βF and βD	hydrophobic

[a] The atomic contacts were deduced from the known X-ray structures as described in Materials and Methods. Residue numbering corresponds to the known sequence numbering. Structurally equivalent contacts are listed on the same line. Conserved residues are indicated in bold.

A similar result has been obtained with Tt IPMDH Trp mutants (Figure 5D) in agreement with the simultaneous and cooperative refolding of protein domains and subunits. This folding mechanism also assumes that the high extent of symmetry has prevailed, starting from the beginning, during the whole process.

It is notable, however, that in the case of the mutant lacking W195 (W152,195F) and possessing a less compact native structure FRET does not appear as a burst upon addition of IPM (as occurred with the wild-type enzyme) but formed in a time-dependent manner (cf. the lower time course in Figure 5C), similar to the time course of the slow phase of refolding from the denatured state of either the wild-type enzyme or any of the other mutants.

Since FRET is indicative of IPM binding, we could use this signal for titration with IPM and determination of the binding constants of this substrate to Tt, Ec, and Vib IPMDHs (Figure 5E). The K_d values of 34.1 ± 2.3, 10.9 ± 0.7, and 1.3 ± 0.1 μM were obtained for the Tt, Ec, and Vib enzymes, respectively. Previously 10.6 μM was determined by Dean and Dvorak under similar conditions for Tt IPMDH (*24*). In the following we could also detect changes in the K_d values of IPM binding during the slow phase of refolding of all Tt, Ec, and Vib enzymes (cf. Materials and Methods and Figure 5F). Extrapolating the obtained time courses plotted in Figure 5F back to its initial phase, we can estimate that IPM binding is relatively strong even at the beginning of the slow part. Thus, one can assume that the early dimeric intermediate is already able to bind IPM, although this initial binding is not a native-like enzyme−substrate interaction, since this species does not exhibit the FRET phenomenon. The binding site of IPM is only fully restored during the slow phase of refolding with the concomitant formation of interdomain and intersubunit interactions, characteristic of the IPM-bound state.

What Is the Structural Basis of the Cooperative Refolding of the Two Domains and the Two Subunits of IPMDH? Surveying the available data in the literature about unfolding−refolding properties of oligomeric proteins, one can find cases when the simple two-state mechanism occurs (i.e., folded oligomer ↔ unfolded monomers) (e.g., refs *36* and *37*). However, mechanisms including the existence of folding intermediates that are either unfolded oligomer (*38–42*) or folded/partially folded monomer (*43–49*) are rather frequent. Among them there are examples when refolding requires preassociation of monomeric subunits, similar to the present finding with IPMDH. Such examples are phosphofructokinase, aspartate−homoserine dehydrogenase, fatty acid synthetase (*38*), bacterial luciferase (*40*), *E. coli* Trp repressor protein (*47*), immunoglobulin light chain assembly (*41*), and β B1 crystalline (*42*). In some cases persuading experimental

results are presented in favor of such a mechanism: genetic fusion of subunits of a dimeric protein substantially enhanced its rate of folding (*39*) or artificially produced monomers that could not refold into a native dimer but only into a nonnative monomer (*46*).

Considering the folding problem of domains, they are originally proposed to be independent folding units in the pathway of a hierarchical folding mechanism (*3*); however, there are examples of folding cooperativity between the domains (e.g., glutathione transferase (*50*)), similar to the mechanism shown for IPMDH.

In spite of the numerous publications, structural background for the occurrence of one or the other mechanism is very rarely given (*47*). Here we attempt to explain the refolding cooperativity on the basis of the structural characteristics of IPMDHs. The molecular contacts at the subunit interfaces and at the domain−domain interfaces are listed in Tables 1 and 2, respectively. It is evident that both in subunit−subunit and in domain−domain contacts the hydrophobic interactions are dominating. Furthermore, these properties are possibly general characteristics of all IPMDH molecules, since they are very similar for all three investigated IPMDHs, independent of their thermal stability. Interaction between the nonpolar residues is known to strengthen the hydrophobic core of the molecule, and indeed, it has been shown for leucine zipper protein that the hydrophobic interactions increase both the folding rate and stability of the protein even in the absence of electrostatic interactions (*51*). Although the number of contacts of the domain bordering elements (e.g., βF) is smaller with the other domain than within its own domain, the domain bordering β-strands (βF and βE) constitute an essential central part of the hydrophobic core of the whole subunit (cf. Figure 1B). This structural architecture is consistent with the observed cooperative behavior of domains during refolding.

In summary, the hydrophobic nature of the extensive molecular contacts at both the subunit−subunit and domain−domain interfaces is most probably responsible for the observed cooperative refolding of the two domains as well as the two subunits of IPMDH. Since the secondary structural elements are formed much faster than the native tertiary structure, cooperative and simultaneous refolding of the two domains as well as the two subunits is justified. Thus, in contrast to an asymmetric folding mechanism, where one of the two subunits or domains serves as a template for folding of the other subunit or domain (*52*), for IPMDH high extent of symmetry during the folding process of the whole dimeric molecule is suggested.

REFERENCES

1. Dill, K. A., Ozkan, S. B., Weikl, T. R., Chodera, J. D., and Voelz, V. A. (2007) The protein folding problem: when will it be solved? *Curr. Opin. Struct. Biol. 17*, 342–346.
2. Matysiak, S., and Clementi, C. (2008) Mapping folding energy landscapes with theory and experiment. *Arch. Biochem. Biophys. 469*, 29–33.
3. Jaenicke, R. (1998) Protein self-organization in vitro and in vivo: partitioning between physical biochemistry and cell biology. *Biol. Chem. 379*, 237–243.
4. Han, J. H., Batey, S., Nickson, A. A., Teichmann, S. A., and Clarke, J. (2007) The folding and evolution of multidomain proteins. *Nat. Rev. Mol. Cell. Biol. 8*, 319–330.
5. Wiebe, W. J., Sheldon, W. M., and Pomeroy, L. R. (1992) Bacterial growth in the cold: evidence for an enhanced substrate requirement. *Appl. Environ. Microbiol. 58*, 359–364.
6. Imada, K., Sato, M., Tanaka, N., Katsube, Y., Matsuura, Y., and Oshima, T. (1991) Three-dimensional structure of a highly thermostable enzyme, 3-isopropylmalate dehydrogenase of *Thermus thermophilus* at 2.2 Å resolution. *J. Mol. Biol. 222*, 725–738.
7. Hurley, J. H., and Dean, A. M. (1994) Structure of 3-isopropylmalate dehydrogenase in complex with NAD^+: ligand-induced loop closing and mechanism for cofactor specificity. *Structure 2*, 1007–1016.
8. Wallon, G., Kryger, G., Lovett, S. T., Oshima, T., Ringe, D., and Petsko, G. A. (1997) Crystal structures of *Escherichia coli* and *Salmonella typhimurium* 3-isopropylmalate dehydrogenase and comparison with their thermophilic counterpart from *Thermus thermophilus*. *J. Mol. Biol. 266*, 1016–1031.
9. Imada, K., Inagaki, K., Matsunami, H., Kawaguchi, H., Tanaka, H., Tanaka, N., and Namba, K. (1998) Structure of 3-isopropylmalate dehydrogenase in complex with 3-isopropylmalate at 2.0 Å resolution: the role of Glu88 in the unique substrate-recognition mechanism. *Structure 6*, 971–982.
10. Singh, R. K., Kefala, G., Janowski, R., Mueller-Dieckmann, C., von Kries, J. P., and Weiss, M. S. (2005) The high-resolution Structure of LeuB (Rv2995c) from *Mycobacterium tuberculosis*. *J. Mol. Biol. 346*, 1–11.
11. Wallon, G., Lovett, S. T., Magyar, C., Svingor, A., Szilágyi, A., Závodszky, P., Ringe, D., and Petsko, G. A. (1997) Sequence and homology model of 3-isopropylmalate dehydrogenase from the psychrotrophic bacterium *Vibrio* sp. I5 suggest reasons for thermal instability. *Protein Eng. 10*, 665–672.
12. Németh, A., Svingor, A., Pocsik, M., Dobó, J., Magyar, C., Szilágyi, A., Gál, P., and Závodszky, P. (2000) Mirror image mutations reveal the significance of an intersubunit ion cluster in the stability of 3-isopropylmalate dehydrogenase. *FEBS Lett. 468*, 48–52.
13. Hori, T., Moriyama, H., Kawaguchi, J., Hayashi-Iwasaki, Y., Oshima, T., and Tanaka, N. (2000) The initial step of the thermal unfolding of 3-isopropylmalate dehydrogenase detected by the temperature-jump Laue method. *Protein Eng. 13*, 527–533.
14. Svingor, A., Kardos, J., Hajdú, I., Németh, A., and Závodszky, P. (2001) A better enzyme to cope with cold. Comparative flexibility studies on psychrotrophic, mesophilic, and thermophilic IPMDHs. *J. Biol. Chem. 276*, 28121–28125.
15. Motono, C., Yamagishi, A., and Oshima, T. (1999) Urea-induced unfolding and conformational stability of 3-isopropylmalate dehydrogenase from the thermophile *Thermus thermophilus* and its mesophilic counterpart from *Escherichia coli*. *Biochemistry 38*, 1332–1337.
16. Motono, C., Oshima, T., and Yamagishi, A. (2001) High thermal stability of 3-isopropylmalate dehydrogenase from *Thermus thermophilus* resulting from low DeltaDeltaC(p) of unfolding. *Protein Eng. 14*, 961–966.
17. Yasugi, M., Amino, M., Suzuki, T., Oshima, T., and Yamagishi, A. (2001) Cold adaptation of the thermophilic enzyme 3-isopropylmalate dehydrogenase. *J. Biochem. (Tokyo) 129*, 477–484.
18. Ohkuri, T., and Yamagishi, A. (2003) Increased thermal stability against irreversible inactivation of 3-isopropylmalate dehydrogenase induced by decreased van der Waals volume at the subunit interface. *Protein Eng. 16*, 615–621.
19. Gráczer, É., Varga, A., Hajdú, I., Melnik, B., Szilágyi, A., Semisotnov, G., Závodszky, P., and Vas, M. (2007) Rates of unfolding, rather than refolding, determine thermal stabilities of thermophilic, mesophilic, and psychrotrophic 3-isopropylmalate dehydrogenases. *Biochemistry 46*, 11536–11549.
20. Hayashi-Iwasaki, Y., Numata, K., Yamagishi, A., Yutani, K., Sakurai, M., Tanaka, N., and Oshima, T. (1996) A stable intermediate in the thermal unfolding process of a chimeric 3-isopropylmalate dehydrogenase between a thermophilic and a mesophilic enzymes. *Protein Sci. 5*, 511–516.
21. Yamada, T., Akutsu, N., Miyazaki, K., Kakinuma, K., Yoshida, M., and Oshima, T. (1990) Purification, catalytic properties, and thermal stability of *threo*-D-3-isopropylmalate dehydrogenase coded by leuB gene from an extreme thermophile, *Thermus thermophilus* strain HB8. *J. Biochem. (Tokyo) 108*, 449–456.
22. Pace, C. N., Vajdos, F., Fee, L., Grimsley, G., and Gray, T. (1995) How to measure and predict the molar absorption coefficient of a protein. *Protein Sci. 4*, 2411–2423.
23. Lakowicz, J. R. (2006) Fluorescence Anisotropy, in *Principles of Fluorescence Spectroscopy* (Lakowicz, J. R., Ed.) Chapter 10, pp 353−382, Springer Science-Business Media, New York.
24. Dean, A. M., and Dvorak, L. (1995) The role of glutamate 87 in the kinetic mechanism of *Thermus thermophilus* isopropylmalate dehydrogenase. *Protein Sci. 4*, 2156–2167.

25. Ornstein, L. (1964) Disc electrophoresis. I. Background and theory. *Ann. N.Y. Acad. Sci. 121*, 321–349.
26. Nagata, C., Moriyama, H., Tanaka, N., Nakasako, M., Yamamoto, M., Ueki, T., and Oshima, T. (1996) Cryocrystallography of 3-isopropylmalate dehydrogenase from *Thermus thermophilus* and its chimeric enzyme. *Acta Crystallogr., Sect. D: Biol. Crystallogr. 52*, 623–630.
27. Garcia, P., Desmadril, M., Minard, P., and Yon, J. M. (1995) Evidence for residual structures in an unfolded form of yeast phosphoglycerate kinase. *Biochemistry 34*, 397–404.
28. Lakshmikanth, G. S., Sridevi, K., Krishnamoorthy, G., and Udgaonkar, J. B. (2001) Structure is lost incrementally during the unfolding of barstar. *Nat. Struct. Biol. 8*, 799–804.
29. Luke, K., and Wittung-Stafshede, P. (2006) Folding and assembly pathways of co-chaperonin proteins 10: origin of bacterial thermostability. *Arch. Biochem. Biophys. 456*, 8–18.
30. Uversky, V. N., Narizhneva, N. V., Kirschstein, S. O., Winter, S., and Lober, G. (1997) Conformational transitions provoked by organic solvents in beta-lactoglobulin: can a molten globule like intermediate be induced by the decrease in dielectric constant? *Folding Des. 2*, 163–172.
31. Szilágyi, A. N., and Vas, M. (1998) Sequential domain refolding of pig muscle 3-phosphoglycerate kinase: kinetic analysis of reactivation. *Folding Des. 3*, 565–575.
32. Liu, Y. M., Feng, S., Zhao, T. J., Ding, X. L., and Yan, Y. B. (2008) The conserved Cys254 plays a crucial role in creatine kinase refolding under non-reduced conditions but not in its activity or stability. *Biochim. Biophys. Acta 1784*, 2071–2078.
33. Garidel, P. (2008) Steady-state intrinsic tryptophan protein fluorescence spectroscopy in pharmaceutical biotechnology. *Specrosc. Eur. 20*, 7–11.
34. Semisotnov, G. V., Anufrieva, E. V., Zikherman, K. K., Kasatkin, S. B., and Ptitsyn, O. B. (1981) Polarized luminescence and mobility of tryptophan residues in polypeptide chains. *Biopolymers 20*, 2287–2309.
35. Steinberg, I. Z. (1971) Long-range nonradiative transfer of electronic excitation energy in proteins and polypeptides. *Annu. Rev. Biochem. 40*, 83–114.
36. Zitzewitz, J. A., Bilsel, O., Luo, J., Jones, B. E., and Matthews, C. R. (1995) Probing the folding mechanism of a leucine zipper peptide by stopped-flow circular dichroism spectroscopy. *Biochemistry 34*, 12812–12819.
37. Ibarra-Molero, B., Makhatadze, G. I., and Matthews, C. R. (2001) Mapping the energy surface for the folding reaction of the coiled-coil peptide GCN4-p1. *Biochemistry 40*, 719–731.
38. Garel, J. R., Martel, A., Muller, K., Ikai, A., Morishima, N., and Sutoh, K. (1984) Role of subunit interactions in the self-assembly of oligomeric proteins. *Adv. Biophys. 18*, 91–113.
39. Liang, H., Sandberg, W. S., and Terwilliger, T. C. (1993) Genetic fusion of subunits of a dimeric protein substantially enhances its stability and rate of folding. *Proc. Natl. Acad. Sci. U.S.A. 90*, 7010–7014.
40. Baldwin, T. O., Ziegler, M. M., Chaffotte, A. F., and Goldberg, M. E. (1993) Contribution of folding steps involving the individual subunits of bacterial luciferase to the assembly of the active heterodimeric enzyme. *J. Biol. Chem. 268*, 10766–10772.
41. Leitzgen, K., Knittler, M. R., and Haas, I. G. (1997) Assembly of immunoglobulin light chains as a prerequisite for secretion. A model for oligomerization-dependent subunit folding. *J. Biol. Chem. 272*, 3117–3123.
42. Koteiche, H. A., Kumar, M. S., and McHaourab, H. S. (2007) Analysis of betaB1-crystallin unfolding equilibrium by spin and fluorescence labeling: evidence of a dimeric intermediate. *FEBS Lett. 581*, 1933–1938.
43. Rudolph, R., Fuchs, I., and Jaenicke, R. (1986) Reassociation of dimeric cytoplasmic malate dehydrogenase is determined by slow and very slow folding reactions. *Biochemistry 25*, 1662–1669.
44. Mann, C. J., and Matthews, C. R. (1993) Structure and stability of an early folding intermediate of *Escherichia coli* trp aporepressor measured by far-UV stopped-flow circular dichroism and 8-anilino-1-naphthalene sulfonate binding. *Biochemistry 32*, 5282–5290.
45. Abu-Soud, H. M., Loftus, M., and Stuehr, D. J. (1995) Subunit dissociation and unfolding of macrophage NO synthase: relationship between enzyme structure, prosthetic group binding, and catalytic function. *Biochemistry 34*, 11167–11175.
46. Shao, X., and Matthews, C. R. (1998) Single-tryptophan mutants of monomeric tryptophan repressor: optical spectroscopy reveals nonnative structure in a model for an early folding intermediate. *Biochemistry 37*, 7850–7858.
47. Gloss, L. M., Simler, B. R., and Matthews, C. R. (2001) Rough energy landscapes in protein folding: dimeric *E. coli* Trp repressor folds through three parallel channels. *J. Mol. Biol. 312*, 1121–1134.
48. Campana, P. T., Moraes, D. I., Monteiro-Moreira, A. C., and Beltramini, L. M. (2002) Unfolding and refolding studies of frutalin, a tetrameric D-galactose binding lectin. *Eur. J. Biochem. 269*, 753–758.
49. Qin, G., Jianwei, Z., Taotao, L., and Xicheng, W. (2007) Intermediates in the refolding of urea-denatured dimeric arginine kinase from *Stichopus japonicus*. *Int. J. Biol. Macromol. 41*, 521–528.
50. Thompson, L. C., Walters, J., Burke, J., Parsons, J. F., Armstrong, R. N., and Dirr, H. W. (2006) Double mutation at the subunit interface of glutathione transferase rGSTM1-1 results in a stable, folded monomer. *Biochemistry 45*, 2267–2273.
51. Durr, E., Jelesarov, I., and Bosshard, H. R. (1999) Extremely fast folding of a very stable leucine zipper with a strengthened hydrophobic core and lacking electrostatic interactions between helices. *Biochemistry 38*, 870–880.
52. Levy, Y., Cho, S. S., Onuchic, J. N., and Wolynes, P. G. (2005) A survey of flexible protein binding mechanisms and their transition states using native topology based energy landscapes. *J. Mol. Biol. 346*, 1121–1145.

BI801857T